Digital Biomarker for Muscle Function Assessment Using Surface Electromyography With Electrical Stimulation and a Non-Invasive Wearable Device

Kwangsub Song, Hyung Eun Shin, Wookhyun Park, Daehyun Lee, Jaeyoung Jang, Ga Yang Shim, Sangui Choi, Miji Kim, Hooman Lee, *Member, IEEE*, and Chang Won Won

***Abstract*— Sarcopenia is a comprehensive degenerative disease with the progressive loss of skeletal muscle mass with age, accompanied by the loss of muscle strength and muscle dysfunction. Individuals with unmanaged sarcopenia may experience adverse outcomes. Periodically monitoring muscle function to detect muscle degeneration caused by sarcopenia and treating degenerated muscles is essential. We proposed a digital biomarker measurement technique using surface electromyography (sEMG) with electrical stimulation and wearable device to conveniently monitor muscle function at home. When motor neurons and muscle fibers are electrically stimulated, stimulated muscle contraction signals (SMCSs) can be obtained using an sEMG sensor. As motor neuron activation is important for muscle contraction and strength, their action potentials for electrical stimulation represent the muscle function. Thus, the SMCSs are closely related to muscle function, presumptively. Using the SMCSs data, a feature vector concatenating spectrogram-based features and deep learning features extracted from a convolutional neural network model using continuous wavelet transform images was used as the input to train a regression model for measuring the digital biomarker. To verify muscle function measurement technique, we recruited 98 healthy participants aged 20–60 years including 48 [49%] men who volunteered for this study. The Pearson correlation coefficient between the label and model estimates was 0.89, suggesting that the proposed model can robustly estimate the label using SMCSs, with mean error and standard deviation of -0.06 and 0.68, respectively. In conclusion, measuring muscle function using the proposed system that involves SMCSs is feasible.**

***Index Terms*— Digital biomarker, muscle mass, muscle strength, stimulated muscle contraction signal, deep neural network.**

Manuscript received 19 December 2023; revised 14 July 2024; accepted 13 August 2024. Date of publication 16 August 2024; date of current version 26 August 2024. This work was supported in part by Korea Medical Device Development Fund Grant funded by Korea Government (the Ministry of Science and Information and Communication Technology (ICT), the Ministry of Trade, Industry and Energy, the Ministry of Health and Welfare, and the Ministry of Food and Drug Safety) under Project RS-2020-KD000101; and in part by the Technology Innovation Program funded by the Ministry of Trade, Industry and Energy (MOTIE), South Korea, under Grant 20018182. *(Corresponding authors: Hooman Lee; Chang Won Won.)*

This work involved human subjects or animals in its research. Approval of all ethical and experimental procedures and protocols was granted by the Clinical Research Ethics Committee of Kyung Hee University Medical Center Institutional Review Board under Application No. 2021-04-065, and performed in line with the Declaration of Helsinki.

Kwangsub Song, Wookhyun Park, Sangui Choi, and Hooman Lee are with the Research and Development Center of Exosystems, Seongnam 13449, Republic of Korea (e-mail: will@exosystems.io; david@exosystems.io; tkddml30@exosystems.io; hoomanlee@exosystems.io).

Hyung Eun Shin, Daehyun Lee, and Jaeyoung Jang are with the Department of Biomedical Science and Technology, Graduate School, Kyung Hee University, Seoul 02447, Republic of Korea (e-mail: she9310@gmail.com; lyh737@naver.com; hustleyoung18@gmail.com).

Ga Yang Shim is with the Department of Physical Medicine and Rehabilitation Medicine, Kyung Hee University Medical Center, Seoul 02447, Republic of Korea (e-mail: wholhear@gmail.com).

Miji Kim is with the Department of Biomedical Science and Technology, College of Medicine, East-West Medical Research Institute, Kyung Hee University, Seoul 02447, Republic of Korea (e-mail: mijiak@khu.ac.kr).

Chang Won Won is with the Elderly Frailty Research Center, Department of Family Medicine, College of Medicine, Kyung Hee University, Kyung Hee University Medical Center, Seoul 02447, Republic of Korea (e-mail: chunwon62@naver.com).

Digital Object Identifier 10.1109/TNSRE.2024.3444890

I. Introduction

SARCOPENIA is a muscle degenerative disorder related to age or disease and is defined as decreased skeletal muscle mass and strength and/or reduced muscle function [1]. Additionally, with muscle degeneration, the condition of the myelin sheath in motor neurons deteriorates and the number of motor neurons and axons decreases with muscle degeneration [2]. Hence, muscle quality, which is a good indicator of muscle function, is impaired by muscle degeneration [3], [4], [5]. As muscle degeneration progresses, decrease in muscle mass occurs after the age of 35 years, and muscle mass and strength steadily reduce. The peak age and rate of decrease in skeletal muscle mass are different for each individual [3], [6]. Muscle degeneration owing to aging or disease, causes a decrease in myofunction [7], thereby increasing the risk of accidents in daily life. With no intervention, falls and fractures may occur due to a balance disorder caused by sarcopenia [8], [9], [10]. Hence, to prevent muscle degeneration the muscle function could be periodically checked to provide appropriate exercise recommendations to patients for improving their muscle health. [11], [12].

Muscle function in patients has been typically measured using the muscle strength test and timed up-and-go test conducted by an expert in the hospital [6], [13], [14]. However, muscle function may not be accurately evaluated by relying solely on muscle strength. Therefore, recent studies have been conducted from the perspective of muscle quality to assess muscle function [15], [16]. The motor unit consists of a motor neuron and the muscle fibers that it innervates through its axon terminals, encompassing the neuromuscular junctions connecting the neuron to the muscle fibers. Muscle motor neurons, muscle fibers, and muscle fiber firing rate play crucial roles in muscle contraction; therefore, their condition is closely related to muscle strength. Although individuals within a certain group may have the same muscle mass, differences in muscle strength can occur based on the structure of their motor units. Therefore, to evaluate motor unit function, we propose a muscle quality index as a digital biomarker (muscle strength/muscle mass).

In addition, accurately measuring muscle strength using professional equipment, such as the microFET and Biodex, is challenging and inconvenient without an expert [17], [18]. Because professional equipment is expensive, patients cannot periodically measure their muscle strength. Also, for older individuals with hypertension, muscle strength test may increase the risk of hemorrhagic stroke [19], [20], [21]. There is an increasing demand for easy and convenient methods to monitor muscle function at home for health promotion [22], [23], [24], [25].

To address these issues, we propose a digital biomarker measurement technique using a wearable device to assess muscle function. To assess muscle function, obtaining information on the condition of the muscle motor neurons, fibers, and fiber firing rate is necessary, as muscle function is closely related to these components. Hence, we recorded the response signals of motor neurons and muscle fibers activated by electrical stimulation, defined as stimulated muscle contractions, using a surface electromyography (sEMG) sensor. The resultant stimulated muscle contraction signal (SMCSs) includes information about motor neurons and muscle fibers but excludes the muscle fiber firing rate. The muscle fiber firing rates observed during voluntary muscle contraction has different characteristics compared to the SMCSs recorded during involuntary muscle contraction induced by electrical stimulation. Moreover, owing to motor neuron and muscle fiber degeneration, the cross-sectional area decreases, leading to impaired muscle function. This affects the response signals of the motor neurons and muscle fibers stimulated by electrical stimulation. Hence, the SMCSs include response signals of the motor neuron and muscle fiber [26] such as M-wave, H-wave, F-wave, and so on, and it includes bioinformation related with the skeletal muscle contraction [27], [28], [29]. Thereafter, we propose a muscle function assessment technique based on an artificial intelligence (AI) model using the SMCSs. First, the signal was processed through feature extraction after the SMCSs were recorded by the EMG sensor. While recording the SMCSs, the sEMG sensor captured the response signals from the motor neurons and muscle fibers, as well as the artifact noise generated by electrical stimulation. To improve the performance of the proposed system, it is necessary to remove the artifact noise. However, because artifact noise occurs almost simultaneously with the response signals from motor neurons and muscle fibers, and the sampling frequency of the sEMG is not high enough to distinguish between them, it is difficult to separate artifact noise from the response signals and removing artifact noise might distort the response signals, the preprocessing step to remove artifact noise was excluded. The input of the AI model consisted of muscle contraction pattern (MCP) features extracted based on spectrograms, continuous wavelet transform (CWT) features extracted based on deep learning, and body information. Finally, we trained the digital biomarker estimation model using an input vector to assess the muscle function. We also attempted to verify the performance of the proposed technique.

II. Technical Concept

A. Stimulated Muscle Contraction Signal (SMCS)

When the sEMG sensor records the myoelectric signal along with voluntary muscle contraction, the relationship between the amplitude of the sEMG and muscle strength is nonlinear [30], [31]. In addition, the results of conventional sEMG tests are influenced by the participant's volition; therefore, objectively determining muscle function is challenging. To address this issue, muscle contraction is induced by electrical stimulation, and the sEMG signal is simultaneously recorded to analyze the MCP, which appears differently according to muscle function (Fig. 1.A). To achieve various biosignals, the SMCSs were collected using various frequency parameters of electrical stimulation. The results are shown in Fig. 1.B; the SMCSs can be transmitted through a mobile device connected by Bluetooth, and the signal passes through the proposed AI algorithm to assess muscle function.

B. System Prototype for Recording SMCSs

As shown in Fig. 1.A, the novel system presented in this study involves an sEMG sensor to record the SMCSs using an electrical stimulation generator installed in the wearable device. The proposed approach consists of a hardware system for recording the SMCSs and a software system for controlling the hardware system. The mobile device is first connected to the cradle and then to the wearable device via Bluetooth, as shown in Fig. 1. The wearable device can be controlled using the recording button of the application on the mobile device. Finally, the SMCSs are saved to the server after the signal is transmitted to the mobile device.

C. Usage

As shown in Fig. 1.A, the electrode pads are attached to the rectus femoris, and the wearable device of the cradle is connected to them via a magnetic button. After the user downloads the application in their device, such as a tablet or smartphone, the they connect the wearable device to it via Bluetooth. While generating the electrical stimulation at the rectus femoris, the user must not move while collecting data. As the algorithm does not require voluntary muscle contraction, which occurs because of the user's volition, the

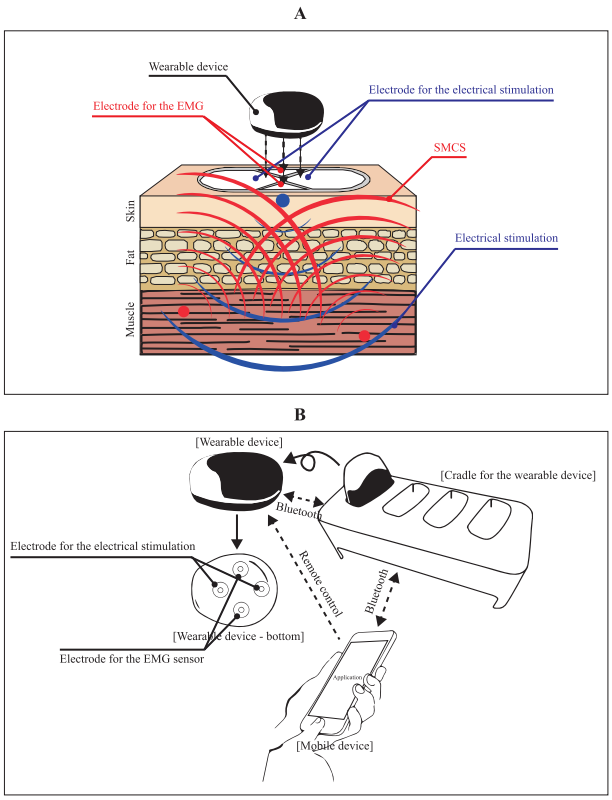

Fig. 1. Concept of the proposed system. (A) Outline of the stimulated muscle contraction signals (SMCSs) data acquisition method. The red and blue lines are related to the surface electromyography (sEMG) sensor and electrical stimulation, respectively. The figure shows the concept of the SMCSs data recording. While the electrical signal stimulates the target muscle, the muscle response signal is recorded by the sEMG sensor in the wearable device, as indicated by the red line. (B) The connection structure to use the wearable device.

user maintains the relaxed state of the muscle after contraction. Finally, when data recording is completed, the data are saved in local storage in the participant's mobile phone or tablet.

III. Materials and Methods

We performed a stability test on the wearable device before the experiment. To minimize the noise that might occur from the electrode pad, one pad was used by one participant when the SMCSs were collected using a wearable device. Because we designed the SMCSs, which was composed of the MCP by electrical stimulation, the muscle contraction signal by volition must not be included in the SMCSs. The clinical researcher observed whether the participants contracted their muscles. If the participant contracted their muscles by volition, we recorded the SMCSs.

A. Hardware Description

Our experimental system consists of a cradle and two modules. The modules generate electrical stimulation signals based on parameters provided by a user application and send the measured EMG signals back to the application. The cradle is responsible for recharging the modules' batteries, providing information about the available modules to the user application, and indicating the operational status of the modules externally.

The modules consist of custom-designed circuits, four electrodes, a bi-colored light-emitting diode (LED), a battery, and charging pins. All components are housed in a self-manufactured polycarbonate case with dimensions of 50 × 59 × 23 mm. The four magnetic electrodes, attached to a hydrogel pad, slightly protrude from the bottom of the case. The charging pins are accessible on the back, and the module weighs approximately 40g. The module is powered by a 3.7V, 250 mAh lithium-ion polymer battery, which is charged with a DC voltage of 4.2V and a current of 450 mAh.

The embedded microprocessor (STM32L451CE, STMicroelectronics) communicates with a Bluetooth low-energy module (NRF52840, Nordic Semiconductor) using UART communication at 115,200 bps. This setup enables the module to receive commands from a user application connected via Bluetooth 5.0 and control the module's circuitry. The circuitry generates an electric stimulation signal consisting of three serial pulse-waveforms (1.40 ms, bi-phased, 50% pulse width) at frequencies ranging from 5 to 100 Hz, with a maximum peak-to-peak amplitude of 100V (measured with a 500 ohm noninductive resistor). This signal is delivered through the stimulation electrodes. The EMG signal, collected by the EMG electrodes, is amplified and filtered through a band-pass filter with cutoff frequencies of 9 and 760 Hz (analog signal conditioning). The microcontroller measures this signal at a rate of 1000 samples per second using 8-bit analog-to-digital conversion and transmits the data to the user application.

The cradle consists of custom-built circuits, LEDs, a flexible numeric display (FND), a piezo-electronic buzzer, charging pins, and a DC jack. All components are enclosed in a self-manufactured polycarbonate case, with a dimension of 189 × 85 × 57 mm. The four pogo pins are exposed on the top, and the 5V DC jack is on the back of the cradle. Weighing approximately 270g, the cradle charges the modules via the pogo pins and operates its embedded microprocessor (STM32F401RE, STMicroelectronics).

The processor interfaces with two Bluetooth low-energy modules (NRF52840, Nordic Semiconductor). One Bluetooth module connects to our experimental modules, monitoring their operational status, while the other awaits a connection from the user application. Both Bluetooth modules use UART communication with the microprocessor at 921,600 bps and 115,200 bps, respectively. The cradle displays the status of the connected modules using LEDs and indicates the operation of our experimental devices by showing numeric texts on the FND and emitting beep sounds through the buzzer, based on commands received from the user application.

B. Software Description

The software process consisted of a data collection stage and a digital biomarker estimation stage. First, for the data collection stage, an Android-based application was created to run on a mobile device, such as a smartphone or tablet. The wearable device connected via Bluetooth to the mobile device then recorded the SMCSs using the application, and the data were saved in local storage.

After removing the offset value from the SMCSs, features were extracted to estimate the digital biomarkers. Six electrical

Algorithm 1 Peak Detection

Goal:

1. i_{P} detection of each frequency bin of the spectrogram
2. i_{N} detection of each frequency bin of the spectrogram

Procedure:

Input is spectrogram $X_{\mathrm{n}}(i, j)$

for $n = 5Hz, \ldots, 30Hz$ **do**
  for $j = 1, \ldots, 32$ **do**
    for i =*2:99* **do**
      if $(X_n(i, j) - X_n(i-1, j) > 0$ *and* $X_n(i+1, j) - X_n(i, j) < 0)$ **then**
        $i_{\mathrm{P}} = i$
    $X_n(i, j) = -X_n(i, j)$
    for i =*2:99* **do**
      if $(X_n(i, j) - X_n(i-1, j) > 0$ *and* $X_n(i+1, j) - X_n(i, j) < 0)$ **then**
        $i_{\mathrm{N}} = i$

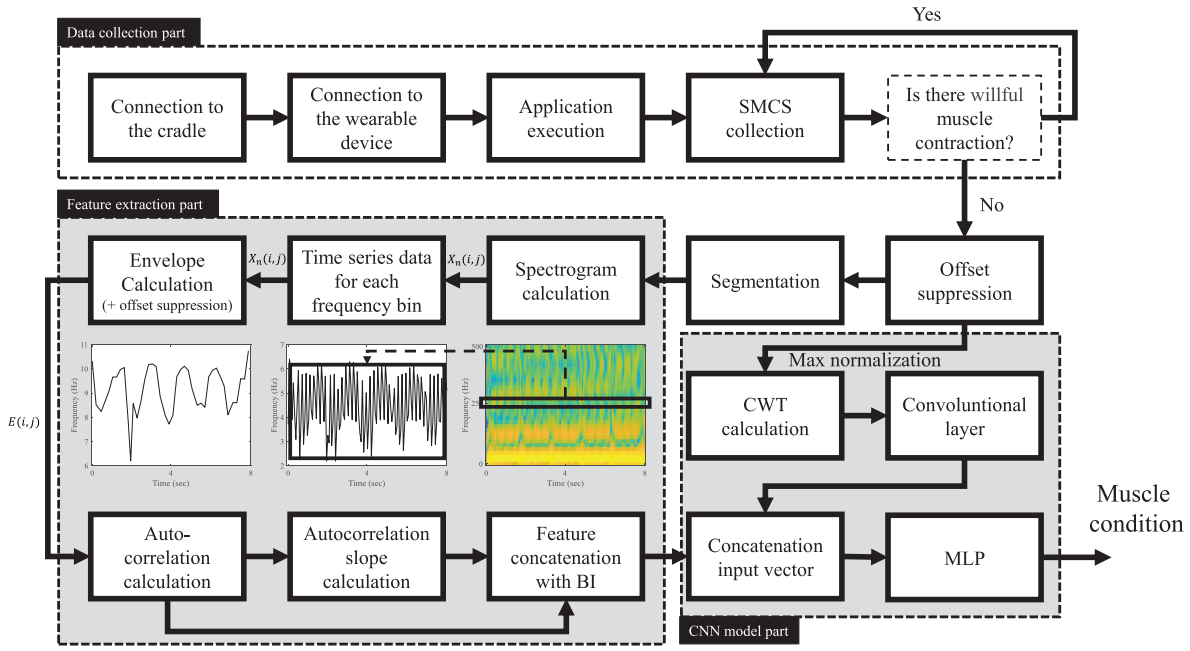

Fig. 2. Complete block diagram of the proposed technique.

stimulation frequencies were used to record the SMCSs, and before extracting features, the SMCSs were divided into six segments based on these frequencies. The feature extraction process, as depicted in Fig. 2, consisted of four stages and was iteratively performed until all segments of the SMCSs were processed. To analyze changes of the frequency components over time in the response signals of the neuromuscular system during electrical stimulation, we then extracted features that could express the MCP through spectrogram analysis. As shown in Fig. 2, the envelope for each frequency bin was calculated after the SMCSs were converted into spectrogram $X_n(i, j)$. The pairs of positive peaks i_{P} and negative peaks i_{N} were added, and the samples between the pairs were interpolated. At this point, the peak detection was performed based on Algorithm 1.

In Algorithm 1, i and j are the frame and frequency-bin indices of the spectrogram, respectively. Additionally, n denotes the frequency of the electrical stimulation. Next, the amplitudes of i_{P} and i_{N} were added, and the samples between the pairs were linearly interpolated, as shown in Fig. 2 [32]. Finally, after the interpolation, the envelope signal E(i,j) was obtained. The offset of the envelope signal was normalized to the mean and standard deviation (SD) of the envelope signal.

$$E(i, j) = (E(i, j) - \boldsymbol{\mu}_E(j))/\boldsymbol{\sigma}_E(j) \tag{1}$$

where $\mu_E(j)$ and $\sigma_E(j)$ represent the mean and SD, respectively, of the extracted envelope for each frequency bin. The autocorrelation of the envelope was calculated to express the MCP, and the outcome value of the autocorrelation function was employed as the feature vector. In addition, the slope

of the autocorrelation was calculated to extract the variation in the MCP. As the offset of the envelope may include essential information, we repeatedly extracted features using an envelope that included the offset. Furthermore, to reduce the feature dimension, features were selected if their absolute correlation with the digital biomarker was > 0.35. Because we carry out three-fold cross validation, the selected features were determined by a voting procedure using all folds. In summary, when each feature was selected from all the folds, it was included in the input vector of the model.

To improve model performance, the input vector was concatenated with a convolutional neural network (CNN)-based feature vector. As shown in Fig. 2, after the SMCSs pass through the CWT procedure, the CWT image was used as the CNN input. To extract the major characteristics from SMCSs, the signal recorded by the first electrical stimulation was transformed using the CWT procedure. Various wavelet functions were available for CWT transformation; however, SMCSs were converted into CWT images using a Gaussian wavelet of order three. Indeed, we tried all other wavelet functions, and the Gaussian wavelet of order three demonstrated the best performance. Its superior performance may be attributed to the selected wavelet function exhibiting a pattern most similar to that of the SMCSs, compared with other wavelet functions. The CWT images were used as inputs for the convolutional layer, from which feature vectors related to digital biomarkers were extracted. The convolutional layer consists of five layers, and the outcome of the final layer was a max-pooling process. The kernel size and stride length were set to 2, and batch normalization was performed between the convolutional layers. The filter dimensions were set as 16, 32, 64, 128, and 256. After the transformed signal passed through the convolutional layers, the output vector of the convolutional layers was concatenated with the MCP features, as shown in Fig. 2. Finally, when feature extraction was complete, the feature vector was combined with the body information for use as the input of the regression model.

The input vector and label digital biomarkers were normalized using the mean and SD to minimize the scale difference between the features [33]. There were two stages in training the multilayer perceptron (MLP) model: parameter initialization and fine-tuning. In the parameter initialization stage, the parameters of the MLP model were randomly initialized with a mean of zero uniform distributions. Fine-tuning was then performed using a back-propagation technique to determine the weight matrix and bias vector obtained during the preceding training stage [34]. Backpropagation was performed to update the weight matrix and bias vector obtained in the previous stage. We employed the exponential linear unit function as the activation function [33], [35] and used the mean squared error as the loss function [33]. The number of hidden layers and units were set to two and (64, 64), respectively. To minimize overfitting, the dropout was set to 0.5 [36], [37]. Finally, the trained model can estimate digital biomarkers using a feedforward procedure. At this point, the output of the model was denormalized to convert the normalized value [33].

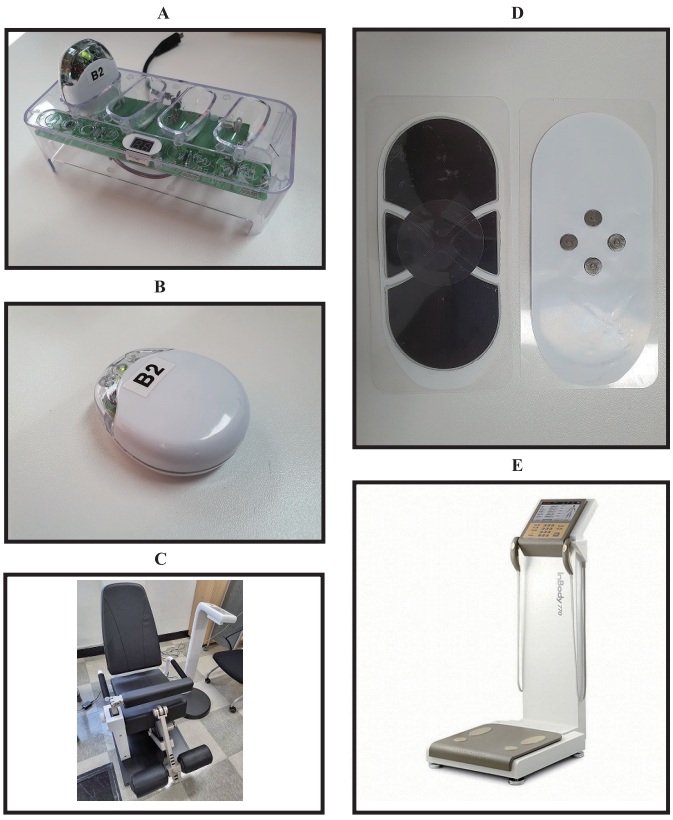

Fig. 3. Photos of the equipment used in the study. (A) Cradle for the wearable device. (B) Wearable device. (C) Equipment for the muscle function test (leg muscle dynamometer). (D) Electrode pad. (E) Bioelectrical impedance analysis equipment.

IV. Experiment Protocol

A. Participants

A total of volunteering 98 participants (community-dwelling adults aged 20–60 years), including 48 (49%) men and 50 (51%) women, were recruited from the Kyung Hee University Medical Center, South Korea, for SMCSs data collection. All participants signed a written consent form. The exclusion criteria were as follows: (1) chronic kidney failure (or end-stage renal disease) or receiving hemodialysis; (2) cancer within the last 5 years or undergoing chemotherapy; (3) receiving hormone therapy; (4) myocardial infarction or stroke in the past 6 months; (5) with a pacemaker; (6) physical disabilities (in the upper or lower limbs); (7) pregnant or breastfeeding women, or planning to become pregnant during the trial period; (8) unable to comply with the study requirements by the investigator's judgement; and (9) low literacy levels.

B. Experimental Equipment and Setup

To collect the SMCSs, the wearable device (ExoPill, Exosystems, Republic of Korea; Fig. 3.A and 3.B) was attached using an electrode pad (StiMus Electrode, HUREV Corp., Republic of Korea; Fig. 3.D) in the rectus femoris as shown in Fig. 4.A, and the EMG sensor, including the SMCSs, was recorded. After the SMCSs were collected using a 5Hz electrical stimulation for 8 s, each participant rested for 2 s. We then collected the signal with the frequency of electrical

TABLE I

THE CLINICAL CHARACTERISTICS OF THE PARTICIPANTS. VALUES ARE PRESENTED AS MEDIANS (25TH AND 75TH PERCENTILES [%]) OR N (%). *p*-VALUES WERE CALCULATED USING THE MANN–WHITNEY TEST FOR CONTINUOUS VARIABLES AND THE CHI-SQUARED TEST OR FISHER'S EXACT TEST FOR CATEGORICAL VARIABLES. TYPES OF DISEASES INCLUDED ALLERGY, RESPIRATORY, CARDIOVASCULAR, GASTROINTESTINAL, LIVER/BILIARY, RENAL/URETHRAL, MUSCULOSKELETAL, METABOLIC/ENDOCRINE, SKIN, REPRODUCTIVE, AND MENTAL/NERVOUS. ABBREVIATIONS: ASMI, APPENDICULAR SKELETAL MUSCLE MASS INDEX; BMI, BODY MASS INDEX

Characteristics	Total (n = 98)	Men (n = 48)	Women (n = 50)	p-values
Age (years)	39.5 (29.0–49.3)	39.0 (29.3–50.8)	39.5 (28.8–48.3)	0.79
Height (cm)	165.8 (161.1–173.6)	173.2 (169.1–178.4)	161.5 (159.7–163.6)	<0.001
Body weight (kg)	61.0 (54.0–71.9)	71.1 (62.3–78.8)	55.2 (50.7–60.2)	<0.001
BMI (kg/cm2)	22.1 (20.4–24.3)	23.5 (21.6–26.0)	21.3 (19.8–22.9)	<0.001
Smoking, n (%)	12 (12.2)	10 (20.8)	2 (4.0)	<0.001
Drinking Alcohol, n (%)	47 (48.0)	28 (58.3)	19 (38.0)	0.068
Diseases past 1-year, n (%)	9 (9.2)	6 (12.5)	3 (6.0)	0.313
ASMI (kg/m2)	7.0 (6.2–8.1)	8.1 (7.5–8.8)	6.3 (5.9–6.7)	<0.001
Right leg muscle mass (kg)	7.2 (6.2–9.3)	9.2 (8.3–10.1)	6.4 (5.9–7.0)	<0.001
Knee-extension force (kg)	39.6 (31.7–55.1)	53.3 (35.3–62.4)	37.0 (29.0–42.8)	<0.001
Knee-flexion force (kg)	28.9 (22.4–35.7)	33.9 (27.7–41.4)	25.1 (19.5–29.3)	<0.001

stimulation set at 10Hz. Finally, we sequentially collected the signal using electrical stimulation at 30Hz. If electrical stimulations at a frequency of 35Hz or higher are used, the intervals between electrical stimulations become too short, making it difficult to observe the response signals of the muscle motor neurons and muscle fibers. Therefore, we limited the maximum electrical stimulation frequency to 30Hz. The SMCSs were recorded for 1 min using a mobile device connected to a wearable device via Bluetooth. To verify the digital biomarker from the SMCSs, we compared the digital biomarker with muscle strength per unit of muscle mass using a leg muscle dynamometer (BS-LS, Inbody, Republic of Korea; Fig. 3.C) for lower limb muscle strength and bioelectrical impedance analysis equipment (Inbody770, Inbody, Republic of Korea; Fig. 3.E) for muscle mass. The equipment was approved as a medical device by the Ministry of Food and Drug Safety in Korea. Muscle strength was determined using the maximum value of the two measurements for each participant.

C. Statistical Analysis

After analyzing the normal distribution using the Kolmogorov– Smirnov test, the Mann–Whitney U test for continuous variables and Fisher's exact test for categorical variables were used to evaluate the characteristics of the participants. To evaluate the performance of the proposed technique, we first trained a deep-learning-based regression model that assessed the quantitative value of muscle function. To validate the performance of the regression model, we used Bland–Altman plots, mean errors (MEs) with SDs, and Pearson's correlation coefficient r-values. We assessed the difference between the estimation results and the labels measured using the reference equipment. All statistical analyses were performed using the SPSS software (version 28.0; SPSS Inc., Chicago, IL, USA) and MATLAB R2020b.

D. Ethics

This study was approved by the Clinical Research Ethics Committee of Kyung Hee University Medical Center (Institutional Review Board number: 2021-04-065), and informed consent was obtained from all participants before data collection.

V. RESULT

A. Experimental Configuration

The clinical characteristics of the participants included in our study are summarized in Table I. The median age was 39.0 years (29.3–50.8 years) for men and 39.5 years (28.8–48.3 years) for women, and this was not significantly different. However, median height (173.2 cm vs. 161.5 cm, $p < 0.001$), body weight (71.1 kg vs. 55.2 kg, $p < 0.001$), and body mass index (23.5 vs. 21.3, $p < 0.001$) were significantly higher in men than in women. In addition, appendicular skeletal muscle mass index (8.1 vs. 6.3, $p < 0.001$), right leg muscle mass (9.2 vs. 6.4, $p < 0.001$), knee extension force (53.3 vs. 37.0, $p < 0.001$), and knee flexion force (33.9 vs. 25.1, $p < 0.001$) were significantly higher in men than in women. Men were more likely to be smokers than women (20.8% vs. 4.0%, $p < 0.001$). To mark the labels for the SMCSs, we used a leg muscle dynamometer for the muscle function test, as shown in Fig. 3.C. We first measured the muscle strength of the lower limb muscles using the equipment and then collected the SMCSs using a wearable device to produce digital biomarkers. Before collecting the SMCSs, the wearable device was validated for reliability and for performance of electrical stimulation and sEMG by the Korea Testing Laboratory (issue number: 23-045628-01-1).

B. Experimental Results

To verify the performance of the proposed technique, the participants were divided into three groups to evaluate the performance of the model using three-fold cross validation. Each fold was assigned as a training, validation, or test set, and experiments were conducted for all combinations. Consequently, the experimental sets were divided into set 1-1, set 1-2, set 2-1,. . ., and set 3-2. The biological structure

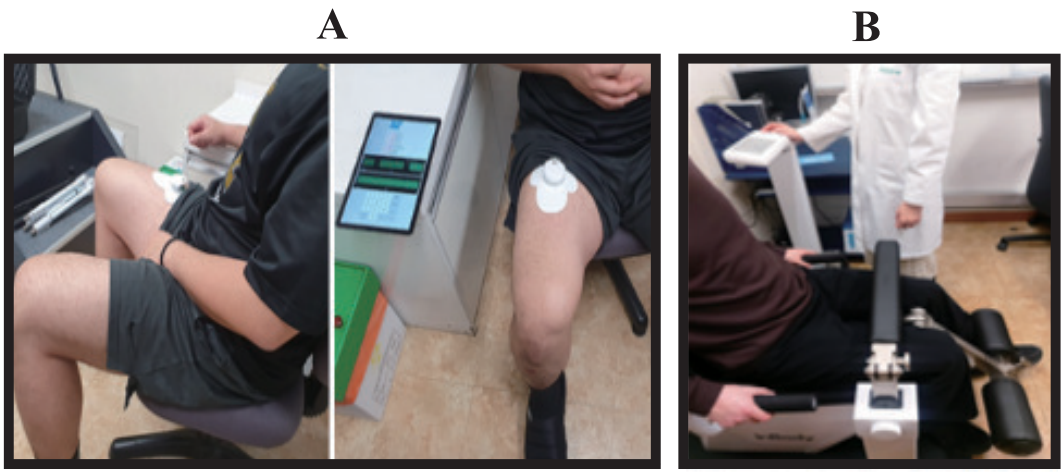

Fig. 4. Photos showing the data collection procedures. (a) Stimulated muscle contraction signals collection. (b) Muscle strength measurement.

TABLE II
PEARSON CORRELATION BETWEEN THE FEATURES AND LABELS FOR THE DIGITAL BIOMARKER TO EVALUATE PERFORMANCE OF THE FEATURES ACCORDING TO SEX AND ELECTRICAL STIMULATION FREQUENCY. PEARSON CORRELATION BETWEEN THE FEATURES AND LABEL WAS EXPRESSED AS THE MEAN VALUE. ABBREVIATIONS: AVG, AVERAGE; SD, STANDARD DEVIATION; MCP, MUSCLE CONTRACTION PATTERN, OE, ORIGINAL ENVELOPE; NE, NORMALIZED ENVELOPE

Type	Gender	MCP						Slope of MCP					
		5Hz	10Hz	15Hz	20Hz	25Hz	30Hz	5Hz	10Hz	15Hz	20Hz	25Hz	30Hz
OE	Male	0.39	0.40	0.54	0.45	0.39	0.51	0.45	0.37	0.44	0.44	0.42	0.45
	Female	0.43	0.42	-	0.41	0.39	0.36	0.47	0.42	0.44	0.44	0.41	0.42
NE	Male	0.40	-	0.47	0.46	0.46	0.46	0.42	0.42	0.42	-	0.44	0.41
	Female	0.45	0.43	0.43	-	0.46	0.44	0.43	0.43	0.43	0.43	0.43	0.43

of muscles differs between women and men; therefore, the proposed model was trained separately for each sex using the proposed method. First, the participants were sorted in descending order based on their label for the digital biomarker, and the participant number was sequentially marked for each participant. To fairly divide the database, the procedure was performed after the database was divided into two groups according to sex. When the operation result of the participant number module three was zero, the participant belonged to the test group, while the remaining were in the training and validation groups. Thus, we performed six experiments for all the cross-validations. In each experiment, the model was ultimately selected when the SD of the error between the model prediction and label was the lowest for training the model for 50 epochs. In addition, because the performance of the model was saturated at 50 epochs, the final epoch of the training model was conducted until the 50th epoch.

Finally, we extracted the feature vector to estimate the digital biomarker and analyzed the correlation between the MCP features and labels for the digital biomarker, as shown in Table II and Appendix. Some of the extracted features were fairly or moderately correlated with digital biomarker labels [38]. Next, to train the CNN model, the SMCSs passed through the CWT procedure, in which the wavelet function was a third-order Gaussian derivative wavelet. To verify the performance of the MLP-based model trained using only MCP features, we verified the MCP feature-based model in which body weight, height, sex, age, and CWT images were not included in the input vector. We then evaluated the performance of the MCP and CWT feature-based models, in which the input vector was constructed using the output of the convolutional layer and MCP features. For all feature-based models, the input vector of the model consisted of body information, MCP features, and the output of the convolutional layer before the MLP layers.

Consequently, all feature-based models, which included body information, MCP features, and the output of the convolutional layer in the input vector, demonstrated the best performance on average. Although the performance of the other models was slightly lower than that of all the feature-based models, the MCP and CWT feature-based models demonstrated stable performances. The experimental results are summarized in Table III and Appendix. As shown in Table III and Appendix, when we compared the MCP and CWT feature-based models with all feature-based models, the SDs and r-values of the MCP and CWT feature-based models were lower than those of all the feature-based models. We also assessed the p-value for the Pearson correlation coefficient to analyze whether there was a statistically significant correlation between the label and model estimation.

Although all feature-based models demonstrated the best performance on average, the MCP and CWT feature-based models were stable for all experimental sets in terms of the SDs and r-values. Fig. 5 shows the scatter and Bland–Altman plots of the estimation results. The scatter plot confirmed that the estimated digital biomarker results and labels for the digital

TABLE III
EVALUATION OF THE MODEL PERFORMANCE BY COMPARING ESTIMATED MODEL VALUES WITH THOSE OF THE DIGITAL BIOMARKER LABEL. ABBREVIATIONS: BI, BODY INFORMATION; ME, MEAN ERROR; STDE, STANDARD DEVIATION OF THE ERROR, CWT; CONTINUOUS WAVELET

	MCP feature-based model			MCP and CWT feature-based model			All feature-based model (including BI)		
	ME	STDE	r-value	ME	STDE	r-value	ME	STDE	r-value
MEAN	0.00	0.81	0.84	0.15	0.74	0.87	-0.06	0.68	0.89
SD	0.07	0.04	0.02	0.13	0.03	0.01	0.17	0.06	0.02

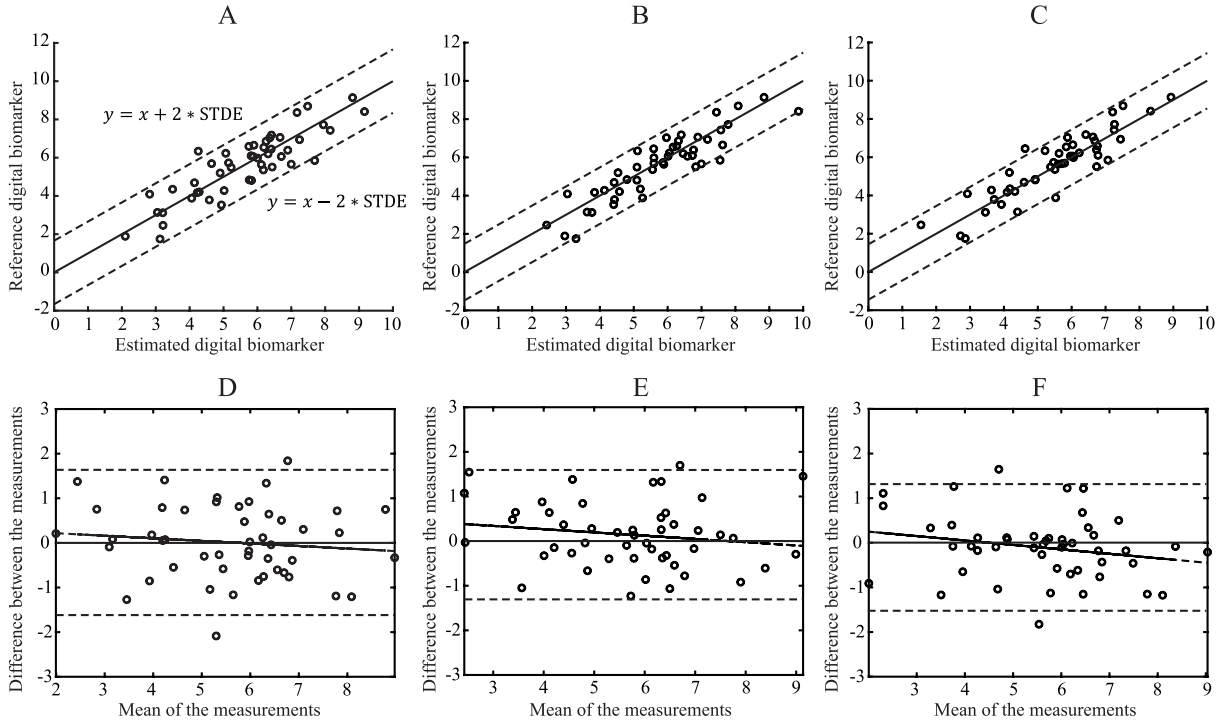

Fig. 5. Experimental results of the regression models for the digital biomarker labels (=muscle strength/muscle mass). The plots show all results of the three-fold cross validation. (a) Scatter plot of the MCP feature-based model (MCP only) results. (b) Scatter plot of the MCP and CWT feature-based model results. (c) Scatter plot of all feature-based model results. (d) Bland–Altman plot of the MCP feature-based model results. (e) Bland–Altman plot of the MCP and CWT feature-based model results. (f) Bland–Altman plot of all feature-based model results. In the Bland–Altman plot, the means of the errors are shown on the x-axis and the differences in the errors are shown on the y-axis. Abbreviations: CWT, continuous wavelet transform; MCP, muscle contraction pattern.

biomarker were highly correlated. Fig. 5.D, 5.E, and 5.F show that the deviation in the model performance was small because of the random distribution of the results of the Bland–Altman plot.

VI. DISCUSSION

We propose a digital biomarker estimation technique to assess muscle function based on the proposed model using the SMCSs. When the muscle was electrically stimulated, the sEMG sensor captured the muscle response signal. To record various pieces of information, an electrical stimulation set was employed at frequencies of 5Hz, 10Hz, 15Hz, 20Hz, 25Hz, and 30Hz. We calculated the spectrum-based muscle response pattern to extract the features of the digital biomarker. We assumed that the MCP produced by electrical stimulation had different characteristics according to the function of each muscle. Consequently, we observed moderate correlation between the features and labels. We trained the regression model based on the CNN using the input vector, including the CWT image, extracted features, and body information, to estimate the digital biomarker. To verify the performance of the proposed model, we conducted three-fold cross validation with objective measurements [39], [40]. For this verification, we analyzed the mean errors (MEs) with SDs of the errors (STDEs), Pearson correlation r-values, and Bland– Altman plots between the assessed and label values. The proposed model demonstrated high performance in terms of the objective measurements. For the three models, the SD of the average STDE in the test database was 0.04, and a low variance between the models was confirmed. Therefore, we confirmed that the models performed fairly well in measuring digital biomarkers. Ultimately, in the proposed system, complex computations such as deep learning and feature extraction are processed on the server side, allowing users to be free from computational burdens. In addition, to confirm the effect of the MCP- and CNN-based CWT features, we trained the

TABLE IV
PEARSON CORRELATION BETWEEN THE FEATURES AND LABELS FOR THE DIGITAL BIOMARKER TO EVALUATE PERFORMANCE OF THE FEATURES ACCORDING TO SEX AND ELECTRICAL STIMULATION FREQUENCY. PEARSON CORRELATION BETWEEN THE FEATURES AND LABEL WAS EXPRESSED AS THE MEAN VALUE. ABBREVIATIONS: AVG, AVERAGE; SD, STANDARD DEVIATION; MCP, MUSCLE CONTRACTION PATTERN, OE, ORIGINAL ENVELOPE; NE, NORMALIZED ENVELOPE

Gender	Statistics	Non-normalization											
		MCP						Slope of MCP					
		5Hz	10Hz	15Hz	20Hz	25Hz	30Hz	5Hz	10Hz	15Hz	20Hz	25Hz	30Hz
Male	AVG	0.39	0.40	0.54	0.45	0.39	0.51	0.45	0.37	0.44	0.44	0.42	0.45
	SD	0.03	0.02	0.06	0.02	0.01	0.01	0.03	0.00	0.06	0.06	0.03	0.03
	MAX	0.42	0.44	0.61	0.48	0.41	0.52	0.49	0.37	0.57	0.52	0.50	0.51
Female	AVG	0.43	0.42	-	0.41	0.39	0.36	0.47	0.42	0.44	0.44	0.41	0.42
	SD	0.02	0.03	-	0.02	0.01	0.01	0.07	0.03	0.05	0.05	0.03	0.04
	MAX	0.45	0.47	-	0.45	0.41	0.37	0.58	0.48	0.55	0.53	0.44	0.51

Gender	Statistics	Normalization											
		MCP						Slope of MCP					
		5Hz	10Hz	15Hz	20Hz	25Hz	30Hz	5Hz	10Hz	15Hz	20Hz	25Hz	30Hz
Male	AVG	0.40	-	0.47	0.46	0.46	0.46	0.42	0.42	0.42	-	0.44	0.41
	SD	0.02	-	0.04	0.01	0.00	0.01	0.03	0.02	0.04	-	0.02	0.03
	MAX	0.43	-	0.52	0.47	0.46	0.47	0.48	0.43	0.47	-	0.46	0.45
Female	AVG	0.45	0.43	0.43	-	0.46	0.44	0.43	0.43	0.43	0.43	0.43	0.43
	SD	0.06	0.04	0.06	-	0.04	0.04	0.05	0.04	0.04	0.00	0.04	0.04
	MAX	0.52	0.51	0.56	-	0.51	0.55	0.50	0.54	0.46	0.43	0.48	0.51

regression model without body information and CNN-based CWT features to confirm the performance of only the MCP features. Although the performance of all feature-based models increased compared with those of the MCP and CWT feature-based models, the MCP and CWT feature-based models could robustly assess muscle function without body information. Thus, all feature-based models exhibited the best performance, and we proved that muscle function can be assessed using the SMCSs.

The electrical stimulation frequency ranged 5–30Hz in increments of 5Hz. To prevent an excessively long data collection period, we increased the electrical stimulation frequency by 5Hz. There may be significant electrical stimulation frequencies between 1Hz and 30Hz that were not used in the study; therefore, further research is required to explore these possibilities.

The proposed system differs from conventional sEMG tests regarding analyzing the response signals of muscle motor neurons and muscle fibers through electrical stimulation. While the conventional sEMG test evaluates noise owing to the influence of the participant's will, the SMCSs collected through the proposed system is significantly mitigated against the influence of will through consistent stimulation. Furthermore, sEMG signals recorded through large-area hydrogel electrodes are complex and difficult to analyze because of the combined action potentials generated by multiple motor units composed of motor neurons and muscle fibers during muscle contraction. To mitigate the issue of signal complexity, previous studies employed high-density (HD) sEMG sensors to analyze muscle conditions quantitatively [41]. HD sEMG sensors with smaller electrode areas can analyze the response signals of fewer motor units than those with larger electrodes, allowing for a relatively accurate analysis. A previous study proposed digital biomarkers to assess muscle aging using HD sEMG sensors and experimentally validated that these biomarkers were related to muscle aging [41]. Analyzing muscle aging quantitatively using conventional sEMG tests was challenging; therefore, the system proposed in the previous study [41] is more desirable than existing methods. This system shared a similar objective with that proposed in this study in terms of mitigating the signal complexity of conventional sEMG tests. In contrast, the system proposed in our study was distinguished by its convenience, as it could be measured without the need for movement, unlike the participants MCP features. Although the performance of all feature-based models increased compared with those of the MCP and CWT feature-based models, the MCP and CWT feature-based models could robustly assess muscle function without body information. Thus, all feature-based models exhibited the best performance, and we proved that muscle function can be assessed using the SMCSs.

The electrical stimulation frequency ranged from 5Hz to 30Hz in increments of 5Hz. To prevent an excessively long

TABLE V
EVALUATION OF THE MODEL PERFORMANCE BY COMPARING ESTIMATED MODEL VALUES WITH THOSE OF THE DIGITAL BIOMARKER LABEL. ABBREVIATIONS: BI, BODY INFORMATION; ME, MEAN ERROR; STDE, STANDARD DEVIATION OF THE ERROR, CWT; CONTINUOUS WAVELET

	Set no.	MCP only (first model)				MCP + CWT (second model)				MCP + CWT + BI (third model)			
		ME	STDE	r-value	p-value	ME	STDE	r-value	p-value	ME	STDE	r-value	p-value
Validation set	Set1-1	0.00	0.75	0.87	<0.001	0.27	0.77	0.87	<0.001	-0.04	0.67	0.90	<0.001
	Set1-2	0.03	0.82	0.83	<0.001	-0.12	0.68	0.88	<0.001	0.02	0.70	0.88	<0.001
	Set2-1	0.15	0.76	0.87	<0.001	0.08	0.80	0.86	<0.001	0.00	0.81	0.85	<0.001
	Set2-2	-0.06	0.73	0.86	<0.001	0.08	0.71	0.87	<0.001	-0.24	0.63	0.90	<0.001
	Set3-1	0.07	0.63	0.91	<0.001	0.28	0.68	0.91	<0.001	-0.11	0.65	0.91	<0.001
	Set3-2	-0.01	0.74	0.88	<0.001	0.10	0.68	0.90	<0.001	0.04	0.76	0.87	<0.001
Statistics	AVG	0.03	0.74	0.87	-	0.12	0.72	0.88	<0.001	-0.06	0.70	0.89	-
	SD	0.07	0.06	0.02	-	0.13	0.05	0.02	<0.001	0.10	0.06	0.02	-
Test set	Set1	0.06	0.80	0.85	<0.001	0.19	0.76	0.87	<0.001	0.18	0.76	0.87	<0.001
	Set2	0.04	0.77	0.86	<0.001	0.29	0.77	0.87	<0.001	-0.11	0.66	0.90	<0.001
	Set3	-0.09	0.86	0.82	<0.001	-0.03	0.69	0.88	<0.001	-0.23	0.62	0.91	<0.001
Statistics	AVG	0.00	0.81	0.84	-	0.15	0.74	0.87	<0.001	-0.06	0.68	0.89	-
	SD	0.07	0.04	0.02	-	0.13	0.03	0.01	<0.001	0.17	0.06	0.02	-

data collection period, we increased the electrical stimulation frequency by 5Hz. There may be significant electrical stimulation frequencies between 1Hz and 30Hz that were not used in the study; therefore, further research is required to explore these possibilities.

The proposed system differs from conventional sEMG tests regarding analyzing the response signals of muscle motor neurons and muscle fibers through electrical stimulation. While the conventional sEMG test evaluates noise owing to the influence of the participant's will, the SMCSs collected through the proposed system is significantly mitigated against the influence of will through consistent stimulation. Furthermore, sEMG signals recorded with large-area hydrogel electrodes were complex and difficult to analyze because of the combined action potentials generated by multiple motor units and the combined signals from motor neurons and muscle fibers during muscle contraction. To mitigate the issue of signal complexity, previous studies used high-density (HD) sEMG sensors to analyze muscle conditions quantitatively [41]. HD sEMG sensors with smaller electrode areas can analyze the response signals of fewer motor units than those with larger electrodes, allowing for a relatively accurate analysis. A previous study proposed digital biomarkers to assess muscle aging using HD sEMG sensors and experimentally validated that these biomarkers were related to muscle aging [41]. Because it is difficult to quantitatively analyze muscle aging using conventional sEMG tests, the system proposed in the previous study [41] is more desirable than existing methods. This system shared a similar objective with that proposed in this study in terms of mitigating the signal complexity of conventional sEMG tests. In contrast, the system proposed in this paper was distinguished by using standardized neuromuscular system bio-signals recorded under the same stimulus, unlike the HD sEMG test. Furthermore, the proposed system is expected to demonstrate high performance if the sEMG sensors used in this study are replaced with the sensors used in the previous study [41]. In this study, we validated the feasibility of the proposed system by collecting the SMCSs data once for each participant. However, further research on the system stability verification should be conducted to observe the performance of the proposed system with repeated measurements for the same participant.

Our proposed technique has several strengths. From a user's perspective, muscle function can be assessed at home without prior knowledge of the equipment. When a medical doctor provides remote care to a patient, the medical doctor can remotely check the muscle function of the patient. From an insurance perspective, if a patient has a muscle-related disease requiring treatment, the patient can use this technique to show how treatment has improved their symptoms, given difficulties in assessing muscle function of patients during short visits. If the patient's condition is poor during the muscle function test, muscle function might be underestimated.

VII. CONCLUSION

In this study, we propose a technique for a digital biomarker for assessing muscle function, by using the SMCSs. We employed the SMCSs to record response signals in our clinical study, and our AI model demonstrated a high correlation between the label and model estimation. In conclusion, the ease and convenience of the proposed technique make it beneficial for patients who may encounter difficulties with mobility and muscle strength measurements.

APPENDIX

The Pearson correlations between the extracted features and the label are summarized in Table II, and more detailed statistical information on the correlation results is summarized in Table IV. The performance of the proposed AI model is

summarized in Table III, and the detailed experimental results are summarized in Table V.

REFERENCES

[1] Y. Feike, L. Zhijie, and C. Wei, "Advances in research on pharmacotherapy of sarcopenia," *Aging Med.*, vol. 4, no. 3, pp. 221–233, Sep. 2021.

[2] M. J. Fogarty and G. C. Sieck, "Aging affects the number and morphological heterogeneity of rat phrenic motor neurons and phrenic motor axons," *Physiol. Rep.*, vol. 11, no. 2, Jan. 2023, Art. no. e15587.

[3] A. J. Cruz-Jentoft and A. A. Sayer, "Sarcopenia," *Lancet*, vol. 393, pp. 2636–2646, Jul. 2019.

[4] J. Xu, C. S. Wan, K. Ktoris, E. M. Reijnierse, and A. B. Maier, "Sarcopenia is associated with mortality in adults: A systematic review and meta-analysis," *Gerontology*, vol. 68, no. 4, pp. 361–376, May 2022.

[5] J. Bauer et al., "Sarcopenia: A time for action. An SCWD position paper," *J. Cachexia, Sarcopenia Muscle*, vol. 10, no. 5, pp. 956–961, Oct. 2019.

[6] A. Tournadre, G. Vial, F. Capel, M. Soubrier, and Y. Boirie, "Sarcopenia," *Joint Bone Spine*, vol. 86, no. 3, pp. 309–314, May 2019.

[7] L.-K. Chen et al., "Asian working group for sarcopenia: 2019 consensus update on sarcopenia diagnosis and treatment," *J. Amer. Med. Directors Assoc.*, vol. 21, no. 3, pp. 300–307, Mar. 2020.

[8] N. Woo and S. H. Kim, "Sarcopenia influences fall-related injuries in community-dwelling older adults," *Geriatric Nursing*, vol. 35, no. 4, pp. 279–282, Jul. 2014.

[9] S. S. Y. Yeung, "Sarcopenia and its association with falls and fractures in older adults: A systematic review and meta-analysis," *J. Cachexia, Sarcopenia Muscle*, vol. 10, pp. 485–500, Jun. 2019.

[10] X. Zhang et al., "Falls among older adults with sarcopenia dwelling in nursing home or community: A meta-analysis," *Clin. Nutrition*, vol. 39, no. 1, pp. 33–39, Jan. 2020.

[11] A. S. Tagliafico, B. Bignotti, L. Torri, and F. Rossi, "Sarcopenia: How to measure, when and why," *La radiologia medica*, vol. 127, no. 3, pp. 228–237, Jan. 2022.

[12] E. Marzetti, "Sarcopenia: An overview," *Aging Clin. Exp. Res.*, vol. 29, pp. 11–17, Feb. 2017.

[13] J. Jung, D.-W. Lee, Y. Son, B. Kim, J. Gu, and H. C. Shin, "Volitional EMG controlled wearable FES system for lower limb rehabilitation," in *Proc. EMBC*, Dec. 2021, pp. 7099–7102.

[14] M. Seifallahi, A. H. Mehraban, J. E. Galvin, and B. Ghoraani, "Alzheimer's disease detection using comprehensive analysis of timed up and go test via Kinect V.2 camera and machine learning," *IEEE Trans. Neural Syst. Rehabil. Eng.*, vol. 30, pp. 1589–1600, 2022.

[15] S. Barbat-Artigas, Y. Rolland, M. Zamboni, and M. Aubertin-Leheudre, "How to assess functional status: A new muscle quality index," *J. Nutrition, Health Aging*, vol. 16, no. 1, pp. 67–77, Jan. 2012.

[16] S. Bastijns, A.-M. De Cock, M. Vandewoude, and S. Perkisas, "Usability and pitfalls of shear-wave elastography for evaluation of muscle quality and its potential in assessing sarcopenia: A review," *Ultrasound Med. Biol.*, vol. 46, no. 11, pp. 2891–2907, Nov. 2020.

[17] T. Voit et al., "Safety and efficacy of drisapersen for the treatment of Duchenne muscular dystrophy (DEMAND II): An exploratory, randomised, placebo-controlled phase 2 study," *Lancet Neurol.*, vol. 13, no. 10, pp. 987–996, Oct. 2014.

[18] H. Nishizawa et al., "Marked motor function improvement in a 32-year-old woman with childhood-onset hypophosphatasia by asfotase alfa therapy: Evaluation based on standardized testing batteries used in Duchenne muscular dystrophy clinical trials," *Mol. Genet. Metabolism Rep.*, vol. 25, Dec. 2020, Art. no. 100643.

[19] J. Dubow and M. E. Fink, "Impact of hypertension on stroke," *Current Atherosclerosis Rep.*, vol. 13, no. 4, pp. 298–305, May 2011.

[20] K. Kario et al., "Morning hypertension: The strongest independent risk factor for stroke in elderly hypertensive patients," *Hypertension Res.*, vol. 29, no. 8, pp. 581–587, Aug. 2006.

[21] S. Kurl, J. A. Laukkanen, R. Rauramaa, T. A. Lakka, J. Sivenius, and J. T. Salonen, "Systolic blood pressure response to exercise stress test and risk of stroke," *Stroke*, vol. 32, no. 9, pp. 2036–2041, Sep. 2001.

[22] S. Rosati et al., "Evaluation of muscle function by means of a muscle-specific and a global index," *Sensors*, vol. 21, no. 21, p. 7186, Oct. 2021.

[23] D. Jiménez-Grande, S. F. Atashzar, E. Martinez-Valdes, and D. Falla, "Muscle network topology analysis for the classification of chronic neck pain based on EMG biomarkers extracted during walking," *PLoS ONE*, vol. 16, no. 6, Jun. 2021, Art. no. e0252657.

[24] I. Hussain and S.-J. Park, "Prediction of myoelectric biomarkers in post-stroke gait," *Sensors*, vol. 21, no. 16, p. 5334, Aug. 2021.

[25] M. Motobe et al., "Noninvasive monitoring of deterioration in skeletal muscle function with forearm cast immobilization and the prevention of deterioration," *Dyn. Med.*, vol. 3, no. 2, pp. 1–11, Feb. 2004.

[26] B. T. H. M. Sleutjes et al., "Impact of stimulus duration on motor unit thresholds and alternation in compound muscle action potential scans," *Clin. Neurophysiol.*, vol. 132, no. 2, pp. 323–331, Feb. 2021.

[27] S. Nakajima and H. Yuminaga, "Approximation of F-wave from evoked electromyography to Poisson distribution and normal distribution," in *Proc. IEEE 2nd Global Conf. Life Sci. Technol. (LifeTech)*, Mar. 2020, pp. 251–252.

[28] K. Nakagawa, K. L. Fok, and K. Masani, "Neuromuscular recruitment pattern in motor point stimulation," *Artif. Organs*, vol. 47, no. 3, pp. 537–546, Mar. 2023.

[29] A. Q. Rana, A. T. Ghouse, and R. Govindarajan, "Essential neurophysiology," in *Neurophysiology in Clinical Practice*, Dec. 2016, pp. 39–50, doi: 10.1007/978-3-319-39342-1_5.

[30] R. Merletti and D. Farina, *Surface Electromyography: Physiology, Engineering, and Applications*. Hoboken, NJ, USA: Wiley, 2016.

[31] K. Watanabe, M. Kouzaki, M. Ogawa, H. Akima, and T. Moritani, "Relationships between muscle strength and multi-channel surface EMG parameters in eighty-eight elderly," *Eur. Rev. Aging Phys. Activity*, vol. 15, no. 1, pp. 1–10, Apr. 2018, doi: 10.1186/s11556-018-0192-z.

[32] M. Forouzanfar, "A modeling approach for coefficient-free oscillometric blood pressure estimation," M.S. thesis, Univ. Ottawa, Ottawa, ON, Canada, 2014. [Online]. Available: https://www.researchgate.net/publication/263808061

[33] K. Song, K.-Y. Chung, and J.-H. Chang, "Cuffless deep learning-based blood pressure estimation for smart wristwatches," *IEEE Trans. Instrum. Meas.*, vol. 69, no. 7, pp. 4292–4302, Jul. 2020.

[34] L. G. Wright et al., "Deep physical neural networks trained with backpropagation," *Nature*, vol. 601, no. 7894, pp. 549–555, Jan. 2022.

[35] H. Alaeddine and M. Jihene, "Deep network in network," *Neural Comput. Appl.*, vol. 33, pp. 1453–1465, May 2020.

[36] F. Yang, H. Zhang, and S. Tao, "Simplified multilayer graph convolutional networks with dropout," *Int. J. Speech Technol.*, vol. 52, no. 5, pp. 4776–4791, Jul. 2021.

[37] J. Pardede, B. Sitohang, S. Akbar, and M. L. Khodra, "Implementation of transfer learning using VGG16 on fruit ripeness detection," *Int. J. Intell. Syst. Appl.*, vol. 13, no. 2, pp. 52–61, Apr. 2021.

[38] H. Akoglu, "User's guide to correlation coefficients," *Turkish J. Emergency Med.*, vol. 18, no. 3, pp. 91–93, Sep. 2018.

[39] A. Ali, S. Ali, M. Husnain, M. M. S. Missen, A. Samad, and M. Khan, "Detection of deficiency of nutrients in grape leaves using deep network," *Math. Problems Eng.*, vol. 2022, pp. 1–12, Jan. 2022, doi: 10.1155/2022/3114525.

[40] N. A. Selamat and S. H. M. Ali, "A novel approach of chewing detection based on temporalis muscle movement using proximity sensor for diet monitoring," in *Proc. IEEE-EMBS Conf. Biomed. Eng. Sci. (IECBES)*, Mar. 2021, pp. 12–17, doi: 10.1109/IECBES48179.2021.9398736.

[41] L. Imrani et al., "High-density surface electromyography as biomarker of muscle aging," *J. Gerontol. A*, vol. 78, no. 1, pp. 25–33, Jul. 2022.